

RESEARCH

Open Access



Ancient bacteria of the Ötzi's microbiome: a genomic tale from the Copper Age

Gabriele Andrea Lugli¹, Christian Milani¹, Leonardo Mancabelli¹, Francesca Turrone¹, Chiara Ferrario¹, Sabrina Duranti¹, Douwe van Sinderen² and Marco Ventura^{1*}

Abstract

Background: Ancient microbiota information represents an important resource to evaluate bacterial evolution and to explore the biological spread of infectious diseases in history. The soft tissue of frozen mummified humans, such as the Tyrolean Iceman, has been shown to contain bacterial DNA that is suitable for population profiling of the prehistoric bacteria that colonized such ancient human hosts.

Results: Here, we performed a microbial cataloging of the distal gut microbiota of the Tyrolean Iceman, which highlights a predominant abundance of *Clostridium* and *Pseudomonas* species. Furthermore, in silico analyses allowed the reconstruction of the genome sequences of five ancient bacterial genomes, including apparent pathogenic ancestor strains of *Clostridium perfringens* and *Pseudomonas veronii* species present in the gut of the Tyrolean Iceman.

Conclusions: Genomic analyses of the reconstructed *C. perfringens* chromosome clearly support the occurrence of a pathogenic profile consisting of virulence genes already existing in the ancient strain, thereby reinforcing the notion of a very early speciation of this taxon towards a pathogenic phenotype. In contrast, the evolutionary development of *P. veronii* appears to be characterized by the acquisition of antibiotic resistance genes in more recent times as well as an evolution towards an ecological niche outside of the (human) gastrointestinal tract.

Keywords: Metagenomics, Genomics, Genomic evolution, Gut bacteria

Background

The (healthy) human gut harbors a highly complex and abundant microbial community (representing bacteria, viruses, and protozoa), also known as the gut microbiota, which exists in an equilibrium with its host [1]. The composition of such a microbiota is markedly influenced by the environment and diet, as well as host's genetics and health status [2]. Since many of the microorganisms harbored by the gastrointestinal tract of animals are considered symbiotic, i.e., their presence is beneficial for both host and microbe, shifts in microbiota composition can exert a substantial impact on the host's physiology. Moreover, disruption of the equilibrium between gut symbionts can lead to colonization of pathogens or overgrowth of opportunistic pathogens, thus causing infectious diseases [3, 4].

In recent years, metagenomic attempts have been carried out to delineate the composition of microbial communities from complex environments such as the human gut [5]. Using Next-generation sequencing (NGS) approaches, it has been possible to investigate the composition of the gut microbiota by sequencing the 16S rRNA marker gene of the bacteria residing in the biological sample, i.e., stool or mucosal biopsy, without the need for microbial cultivation [6–8]. Similar approaches have been applied to characterize the microbiota composition of ancient biological samples retrieved from mummies [9–11]. Several types of ancient specimens, including both coprolites as well as human remains, have been studied during recent years in order to elucidate their microbial associations [11, 12]. In this context, the oral cavity [13, 14] and distal gut microbiota have been extensively analyzed [9, 10]. Notably, depending on climate and storage conditions, genomic data retrieved from ancient biological samples may be inaccurate, due to post-mortem bacterial community alterations [11, 15]. Nevertheless, sufficiently low temperatures such as

* Correspondence: marco.ventura@unipr.it

¹Laboratory of Probiogenomics, Department of Life Sciences, University of Parma, Parco Area delle Scienze 11a, 43124 Parma, Italy

Full list of author information is available at the end of the article



permafrost are believed to represent the optimal conditions for long-term DNA conservation of ancient DNA [16] and for the prevention of post-mortem shifts of bacterial community profiles [17]. In this context, it has recently been showed that when the remains of a deceased are kept at 4 °C, it will take more than 5 days before significant post-mortem bacterial community alterations are observed [18]. This finding suggests that the environmental temperature plays a key role in the stability of post-mortem gut microbiota composition.

Ancient microbiota data sets represent an important source of information that may facilitate the reconstruction of bacterial evolution. Furthermore, collected ancient microbial DNA information may be employed to explore the biological causes and frequency of infectious diseases in history as recently performed for the identification of ancient bacterial pathogens in mummified humans [19–21]. Finally, in recent years, the combination of DNA enrichment methodologies and NGS has enabled researchers to completely reconstruct ancient genomes like those of the pathogens *Yersinia pestis* [19], *Mycobacterium leprae* [20], and *Helicobacter pylori* [21].

The best known frozen and mummified human body, called Ötzi, also referred to as the Tyrolean Iceman, was found in an Italian Alpine glacier [22]. The well-preserved body of Ötzi allowed the retrieval of biological samples from various anatomical regions of this ancient human being [23–25]. A first insight into Ötzi's microbiota composition was obtained from his stomach and colon contents [10]. Recently, an accurate screening of the stomach samples allowed the reconstruction of the genome of the pathogen *H. pylori*, while it also permitted the study of its relatedness to modern *H. pylori* strains retrieved from around the globe [21].

In this study, we performed an in depth metagenomic analysis based on data derived from four biopsy samples recently retrieved from the small and large intestines of the Tyrolean Iceman [21], in an attempt to reconstruct the dominant microbial genomes that constitute the Tyrolean Iceman's distal gut microbiome.

Methods

Genome sequences and metagenome samples

We retrieved complete and partial genome sequences of 20 *Clostridium* and 90 *Pseudomonas* strains from the National Center for Biotechnology Information (NCBI) public database (Additional file 1: Table S1). Illumina HiSeq 2000 paired-end sequencing data of the Tyrolean Iceman gut were retrieved from the European Nucleotide Archive under accession ERP012908 (Additional file 1: Table S2).

Ancient DNA extraction and Illumina libraries preparation

Analyses were performed involving DNA samples processed at the "ancient DNA" Laboratory of the EURAC-

Institute for Mummies and the Iceman, Bolzano, Italy as previously described [21]. Sample preparation and DNA extraction were performed in a dedicated pre-PCR area following the strict procedures required for studies of ancient DNA, which involved the use of protective clothing, UV-light exposure of the equipment and bleach sterilization of surfaces, use of PCR workstations, and filtered pipette tips. DNA extraction was performed with approximately 40 mg of stomach mucosa tissue and 250 mg of gastrointestinal tract content samples using a chloroform-based DNA extraction method according to the protocol of Tang et al. [26]. Negative controls for all experimental steps were included to rule out contamination. DNA was extracted from 100 mg of soft tissue by a magnetic bead-based technology using the Biorobot®-EZ1 (Qiagen, Hilden, Germany), following a previously described procedure [27].

Library preparation and sequencing were performed in DNA-free benches in separate rooms dedicated to aDNA procedures at Kiel University. Libraries for the Illumina runs with the IDs A1140, A1141, A1142, A1144, A1145, and A1146 were prepared from 50 µl of each DNA extract using the Truseq Kit v2.0 (Illumina) and the adapters AD001-AD012, following the manufacturer's protocol. For all purification steps, the Qiaquick Kit (Qiagen, Hilden, Germany) was applied according to the manufacturer's protocol.

Libraries for the sequencing runs were generated from 20 µl of each aDNA extract applying a modified protocol for Illumina multiplex sequencing [28, 29]. For the samples as well as all extraction and library blank controls, unique indexes were added to both library adapters [28]. A second amplification was performed for all indexed libraries in a 50-µl reaction containing 5 µl library template, 2 U AccuPrime Pfx DNA polymerase (Invitrogen), 1 U 10× PCR Mix and 0.3 µM of each primer IS5 and IS6 [29]. The following thermal profile was used: a 2-min initial denaturation at 95 °C, 3, 4, or 8 cycles consisting of 15 s denaturation at 95 °C, a 30-s annealing at 60 °C and a 2-min elongation at 68 °C, and as a final step at the end of the cycles a 5-min elongation at 68 °C. The amplified libraries were purified using the Qiaquick Kit (Qiagen, Hilden, Germany). Subsequently, the sequencing libraries were quantified with the Agilent 2100 Bioanalyzer DNA 1000 chip. The sequencing was carried out on the Illumina HiSeq 2000 and 2500 platform at the Institute of Clinical Molecular Biology, Kiel University, by 2 × 101 cycles using the HiSeq v3 chemistry and the manufacturer's protocol for multiplex sequencing.

Metagenome assemblies

Fastq files of the paired-end reads obtained from shotgun sequencing of the Tyrolean Iceman's small and large intestines, i.e., B0625 (lower part of the large intestine), C1824

and C1825 (upper part of the large intestine), and B0621 (small intestine) (Additional file 1: Table S2) were used as input for the genome assemblies through the MEGAnnotator pipeline [30]. The SPAdes program (version 3.5) was used for de novo metagenomic assemblies [31].

Ancient DNA pattern identification

The mapped reads obtained from a selection of the most abundant bacterial species colonizing the Ötzi's gut were used to confirm their belonging to ancient microorganisms. The selected reads were mapped to their reference genomes (Table 1) in order to assess possible nucleotide mis-incorporation patterns along the DNA fragments. The resulting bam files from the read alignments were checked for ancient DNA patterns using mapDamage [32] in order to depict the C to T mis-incorporation pattern at the 5' end of the reads.

Validation of the CoCla pipeline

Contig Classifier (CoCla) script validation was performed through reconstruction of the ancient genome of *H. pylori* from the 15 *H. pylori*-enriched samples collected from Ötzi's stomach. Alignment of the ancient *H. pylori* and the reference strain *H. pylori* 26695 was performed using Mauve software [33]. Furthermore, the BBmap software (sourceforge.net/projects/bbmap/) has been used to detect chimeric contigs through GC content/coverage plot evaluation.

Metagenome contig selection

After a preliminary assembly with SPAdes [31], each metagenomic sample was analyzed with a customized pipeline aimed at grouping contigs that belong to the same bacterial species. In order to taxonomically classify contigs, open reading frames (ORFs) were predicted with Prodigal [34] and annotated by means of the NCBI database and the aligner RAPSearch2 (cutoff *E* value of 1×10^{-30}) [35]. Taxonomy information of the best hit obtained for each predicted ORF is used by the CoCla

script for contig taxonomy classification based on the most frequently identified microbial species when at least 25% of the ORFs predicted in a contig are attributed to the same species (<http://probiogenomics.unipr.it/sw/CoCla.zip>). Furthermore, we selected those reads from each shotgun metagenomics dataset that were predicted to belong to a particular bacterial species for which a high-quality and high-coverage assembly was obtained. To achieve this selection, for each metagenomics dataset, the pool of reads was mapped with BBmap (minratio = 0.9 maxindel = 3 minhits = 2 qtrim = r trimq = 10 kfilter = 25 maxsites = 1) (sourceforge.net/projects/bbmap/) on all the assembled contigs as well as publicly available sequences of the selected species. All mapped reads were collected and reassembled with SPAdes in order to obtain high-quality assemblies of a specific species that was shown to be abundantly present in the four metagenomics samples analyzed.

Sequence annotation

ORFs were predicted using Prodigal [34]. Transfer RNA genes were identified using tRNAscan-SE v1.4 [36], while ribosomal RNA genes were detected using RNAmmer v1.2 [37]. Results of the gene-finder program were combined with data from RAPSearch2 analysis (Reduced Alphabet based Protein similarity Search) [35] of a non-redundant protein database provided by the National Center for Biotechnology Information (NCBI) and Hidden Markov Model profile (HMM) search (<http://hmmer.org/>) in the manually curated Pfam-A protein family database [38]. The combined results were analyzed through Artemis [39], which was used for a manual-editing effort aimed at verifying and, if necessary, redefining the start of each predicted coding region, to remove or add coding regions, and to discard small ORFs at the edge of the contigs as well as contigs less than 500 bp in length.

Table 1 Ancient genome features

Species	Strain	Genome size	ORFs number	GC content	Contigs	COGs ^a	Core genes ^a	Unique genes ^a	ANI ^b	Related strain
<i>Clostridium</i> sp.	CADE	2,713,669	2605	27.06	333	3,119	1,993	215	90.04	<i>Clostridium</i> sp. Ade.TY
<i>Clostridium algidicarnis</i>	CALG	2,793,371	2588	29.98	95	2,902	2,295	216	98.38	<i>Clostridium algidicarnis</i> B3
<i>Clostridium perfringens</i>	CPER	3,860,191	3739	27.72	1,018	7,720	1,737	493	98.46	<i>Clostridium perfringens</i> SM101
<i>Pseudomonas fluorescens</i>	PFLU	5,806,496	5839	59.05	1,486	33,938	1,627	785	87.4	<i>Pseudomonas fluorescens</i> H14
<i>Pseudomonas syringae</i>	PSYR	2,744,354	2771	57.44	642	–	–	–	–	–
<i>Pseudomonas veronii</i>	PVER	6,299,241	5805	60.49	289	8,700	4,200	615	93.89	<i>Pseudomonas veronii</i> R4

^aData obtained through pan-genome analyses with the public available sequenced genomes of the same species

^bAverage nucleotide identity of the whole sequenced strains

Pan-genome and identification of shared and unique genes

The pan-genome calculation was performed using the PGAP pipeline [40]. The ORF content of all genomes was organized in functional gene clusters using the GF (Gene Family) method involving comparison of each protein to all other proteins using BLAST analysis (cutoff E value of 1×10^{-5} and 50% identity across at least 50% of both protein sequences), followed by clustering into protein families, named clusters of orthologous genes (COGs), using MCL (graph-theory-based Markov clustering algorithm) [41]. A pan-genome profile was built using an optimized algorithm incorporated in PGAP software, based on a presence/absence matrix that included all identified COGs in the analyzed genomes. Following this, the unique protein families for each genome were classified. Protein families shared between all genomes, named core COGs, were defined by selecting the families that contained at least one single protein member for each genome.

Phylogenetic and phylogenomic comparisons

The concatenated core genome sequences were aligned using MAFFT [42], and phylogenetic trees were constructed using the neighbor-joining method in Clustal W, version 2.1 [43]. The core genome supertree was built using FigTree (<http://tree.bio.ed.ac.uk/software/figtree/>). For each genome pair, a value for the average nucleotide identity (ANI) was calculated using the software program JSpecies, version 1.2.1 [44].

Gene gain/loss through evolution reconstruction

Acquisition and loss of genes through evolution of the bacterial species with at least four available genomes was performed with Count software [45] using Dollo's parsimony.

Evaluation of genome sequences and gene distributions

Whole genome sequence alignments for genome coverage analysis were performed at DNA level using LAST (<http://last.cbrc.jp/>). Prediction of the antibiotic resistance determinants were performed with Rapsearch against a custom database and the Transporter Classification Database (TCDB) (cutoff E value of 1×10^{-30} and minimum alignment length 50 nucleotides) [46]. The identification of putative virulence genes was carried out by employing the Virulence Factors Database (VFDB) (cutoff E value of 1×10^{-30} and minimum alignment length 50 nucleotides) [47]. In silico identification of α , β , ϵ , and ι *C. perfringens* toxins were performed using a custom database based on NCBI RefSeq gene sequences.

Functional analyses

The prediction of genes that possess structurally related catalytic and carbohydrate-binding modules of enzyme

that degrade, modify, or create glycosidic bounds were performed through the CAZy database [48]. A survey of the complete pathways involved in both primary and secondary metabolism has been performed by means of the MetaCyc metabolic pathways database [49]. Each collected gene retrieved from NCBI genomes and the reconstructed ones were taken in account for the screenings using a cutoff E value of 1×10^{-10} to identify the best hit from each database.

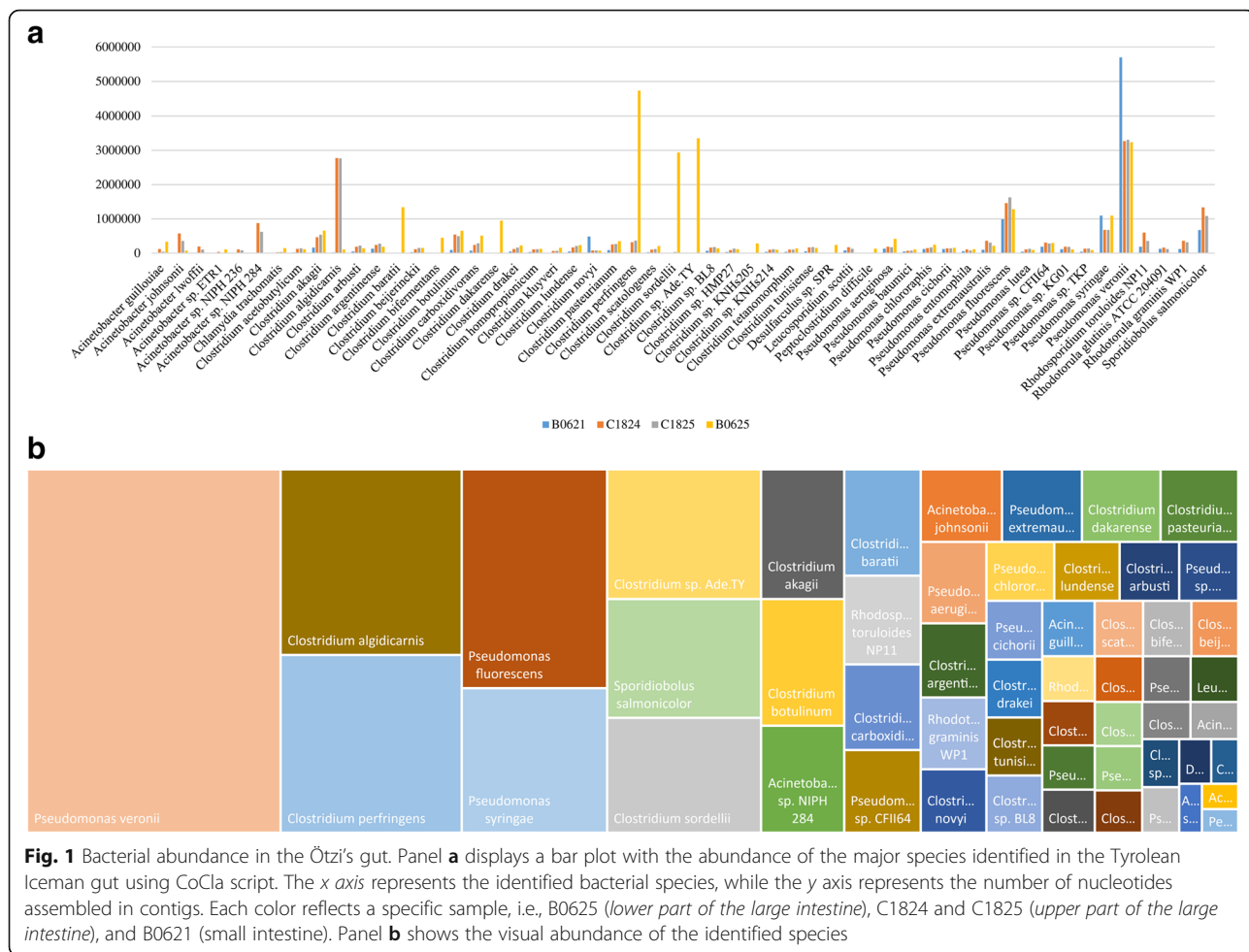
Taxonomic cataloging of bacteria

Taxonomic classification of reads was obtained using RAPSearch2 software [35] for sequence homology in the NCBI nr database, followed by data processing using MEGAN5 software [50].

Results and discussion

Ötzi distal gut microbiome composition

The substantial amount of available sequence data, i.e., 71 gigabases, from the 12 biopsy samples of the gastrointestinal tract of Ötzi has not yet been fully scrutinized and thus represents an intriguing opportunity for further, in depth functional and genomic studies of the ancient microbiota harbored by the Tyrolean Iceman [21]. Notably, these shotgun data were obtained using protocols specific for processing of ancient DNA and executed in a dedicated facilitate so as to prevent the introduction of any contaminating sequences (see "Methods" section for details). Using the CoCla script, we were able to assemble the four intestinal shotgun metagenomic datasets and to elucidate the overall composition of the reconstructed microbiome down to species level. Notably, a substantial proportion of shotgun sequencing data in the samples was predicted to belong to *Pseudomonas veronii* (13.9%) and *Clostridium aldicarnis* (5.1%) species, followed by *Pseudomonas fluorescens* (4.8%), *Clostridium perfringens* (4%), *Pseudomonas syringae* (3.2%) and *Clostridium* sp. Ade.TY (3%) taxa (Additional file 1: Table S3). Interestingly, samples from the lower part of the large intestine (sample B0625) showed a predominant abundance in *Clostridium* species, while samples from the upper part of the large intestine and the small intestine (C1824, C1825, and B0621) produced sequence data that indicated an abundance of *Pseudomonas* species (Fig. 1). Notably, while clostridia are typical inhabitants of the distal intestine [1], often linked to pathologic conditions [4], *P. fluorescens* is typically found in the soil except for specific conditions such as inflammatory bowel disease [51, 52]. In order to validate the functionality of our customized script, we performed an identity sequence analysis based on the reads retrieved from the Ötzi metagenome samples. The resulting information, following a processing step by MEGAN5 software, revealed an abundance of reads belonging to *C. perfringens* in the lower part of the large intestine, or



belonging to *P. fluorescens* in the other three samples from the upper part of the large intestine (Additional file 2: Figure S1). This analysis therefore generated interesting metagenomic data which allowed the genomic reconstruction of the identified prehistoric bacterial species.

In order to evaluate the percentage of the ancient genomes that were covered through targeted genome reconstruction, the obtained contigs were aligned to reference genomes retrieved from the NCBI database. Such analysis showed high coverage (>74.7%) of the *Clostridium* sp. Ade.TY, *C. algidicarnis*, *C. perfringens*, *P. fluorescens*, and *P. veronii* genomes. In contrast, *P. syringae* displayed only a partial coverage (34.1%) of the genome and for this reason was omitted from further analyses (Table 1).

Validation of ancient bacterial DNA origin and identification of putative microbial contaminants

It has been described that bacterial DNA extracted from ancient samples may be compromised by contamination [53]. In order to verify that the genomes that we

reconstructed from Otzi samples are truly of an ancient origin, we performed a sequence damage analysis using the mapDamage software [32]. As shown in Additional file 3: Figure S2, *Clostridium* sp. ADE, *C. algidicarnis* CALG, *C. perfringens* CPER, and *P. veronii* PVER reads display an increased C to T mis-incorporation pattern towards their 5' end (from 5.7 to 9%), indicative of ancient DNA. In contrast, *P. fluorescens* PFLU shows a substantially lower substitution pattern (3.3%), suggesting that this reconstructed genome originated as a DNA contamination of a modern *P. fluorescens*.

Validation of the CoCla pipeline for assembly of ancient DNA and screening for chimeric contigs

The script CoCla was evaluated for read selection reliability and assembly performance when it is employed to process ancient DNA. The 15 *H. pylori*-enriched shotgun datasets retrieved from the stomach of Ötzi were used to reconstruct the ancient *H. pylori* genome and its coverage with respect to the modern strain *H. pylori* 26695. The results from this analysis were then

compared to those obtained by Maixner et al. [21]. Notably, while Maixner et al. achieved an overall genome coverage that ranged from 84.4 to 92.1%, when aligning reads to the reference genome *H. pylori* 26695 [21], the reconstructed ancient genome of *H. pylori* obtained through CoCla pipeline showed a coverage of 92.4% (Additional file 4: Figure S3). Moreover, BBmap software was used for the screening of chimeric contigs, i.e., assembled sequences encompassing exogenous DNA. The results, reported in Additional file 5: Figure S4, highlight the presence of a single cluster in CG content/coverage plots of all the ancient species assembled, thus indicating the (near) absence of alien DNA.

Genomic comparisons of the reconstructed bacterial chromosomes with the currently known microbial genomes

Investigation of the general genome features of the reconstructed chromosomes displayed a genome size ranging from 2,713,669 (*Clostridium* sp. CADE) to 6,299,241 (*P. veronii* PVER), corresponding to 2605 and 5805 predicted protein-encoding genes, respectively (Table 1). Furthermore, the average nucleotide identity (ANI) was estimated between each genome belonging to the same species in order to verify the taxonomic classification of the reconstructed ancient genomes and to evaluate their divergence from “modern” strains [54]. Two of the assembled genomes exhibit an ANI value higher than 96% when compared with publicly available genome sequences of the same species, which represent recent isolates, e.g., *C. algidicarnis* B3-*C. algidicarnis* CALG (98.38%), and *C. perfringens* SM101-*C. perfringens* CPER (98.46%) pairs. The *P. veronii* PVER genome exhibits an average borderline ANI value of 93.89% with four publicly available *P. veronii* strains (Table 1). In contrast, the reconstructed genomes of *Clostridium* sp. CADE display an ANI value of 90.04% when aligned with the chromosome of *Clostridium* sp. Ade.TY. Thus, the ancient *Clostridium* sp. CADE may be considered a new *Clostridium* taxon, possibly representing the ancestor of the currently existing *Clostridium* sp. Ade.TY.

Ancient genome evolution through phylogenomic analysis

The availability of the reconstructed genomes harbored in Ötzi's gut allowed us to obtain insights into the genetic makeup of these ancient bacterial strains. The reconstructed ancient genomes were compared to all publicly available genomic sequences belonging to the same species. In order to reduce the bias caused by different analytical genome pipelines, all genomes retrieved from the NCBI database were processed through the same annotation pipeline adopted for the ancient microbial genomes assembled as part of the current study. Notably, as shown in Table 1, core genome analyses highlight a pool of core genes for each identified species

ranging from 1737 to 4200 for *C. perfringens* and *P. veronii*, respectively. In order to study the phylogenetic relatedness between the reconstructed ancient genomes and the modern ones, the shared core genome-encoded amino acid sequences were compared. Only the species possessing at least four sequenced genomes in the NCBI database were evaluated. Thus, we excluded from this analysis the genomes of *Clostridium* sp. CADE and *C. algidicarnis* CALG. A concatenated protein sequence based on 1570 of the core CperCOGs (*C. perfringens*-specific clusters of orthologous genes), excluding the duplicated genes that appear to be paralogs, was built for the *C. perfringens* species (Fig. 2). In a similar manner, 3629 PverCOGs (*P. veronii*-specific clusters of orthologous genes) were selected in order to design an analogous supertree for the *P. veronii* species (Fig. 2). Those core COG collections represent the most updated core genome sequences of the *C. perfringens* and *P. veronii* species, and from these, a robust reconstruction of the species phylogeny can be inferred [55, 56]. Investigation of the generated phylogenomic results showed that the *P. veronii* supertree constitutes a single branch, while the *C. perfringens* supertree displayed two major branches (Fig. 2).

Interestingly, the ancient genome of *C. perfringens* CPER shares the same phylogenetic branch with the enterotoxin-producing food poisoning strain SM101, a transformable derivative of *C. perfringens* NCTC 8798 [57]. This discovery, together with the high ANI values observed with *C. perfringens* SM101 (98.46), suggests that *C. perfringens* CPER is a human food poisoning strain related to the well-characterized modern strains. Furthermore, the reconstructed *P. veronii* PVER genome does not share the same branch of the other four sequenced *P. veronii* strains, showing a higher degree of sequence variation within its core genome. These observations suggest that only *C. perfringens* CPER possesses a core genome that can be directly compared with a contemporary genome of the same species, while *P. veronii* PVER appears to have a genomic composition that is specific and different compared to that of modern strains. These data are probably linked to the observation that the ancient strain of *P. veronii* PVER seems to have colonized Ötzi's gut, while the modern ones have been isolated from natural mineral water springs [58]. Notably, while we cannot completely exclude that the colonization of Ötzi's large intestine by *P. veronii* PVER may have derived from post-mortem environmental contamination, its abundance and the presence of modern strains in springs may also be due to post-mortem overgrowth of a resident or transient *P. veronii* PVER that had a dietary origin.

Genome evolution trends in modern vs. ancient genomes

In order to evaluate the presence of horizontal gene transfer events (HGT), all genes were classified by a

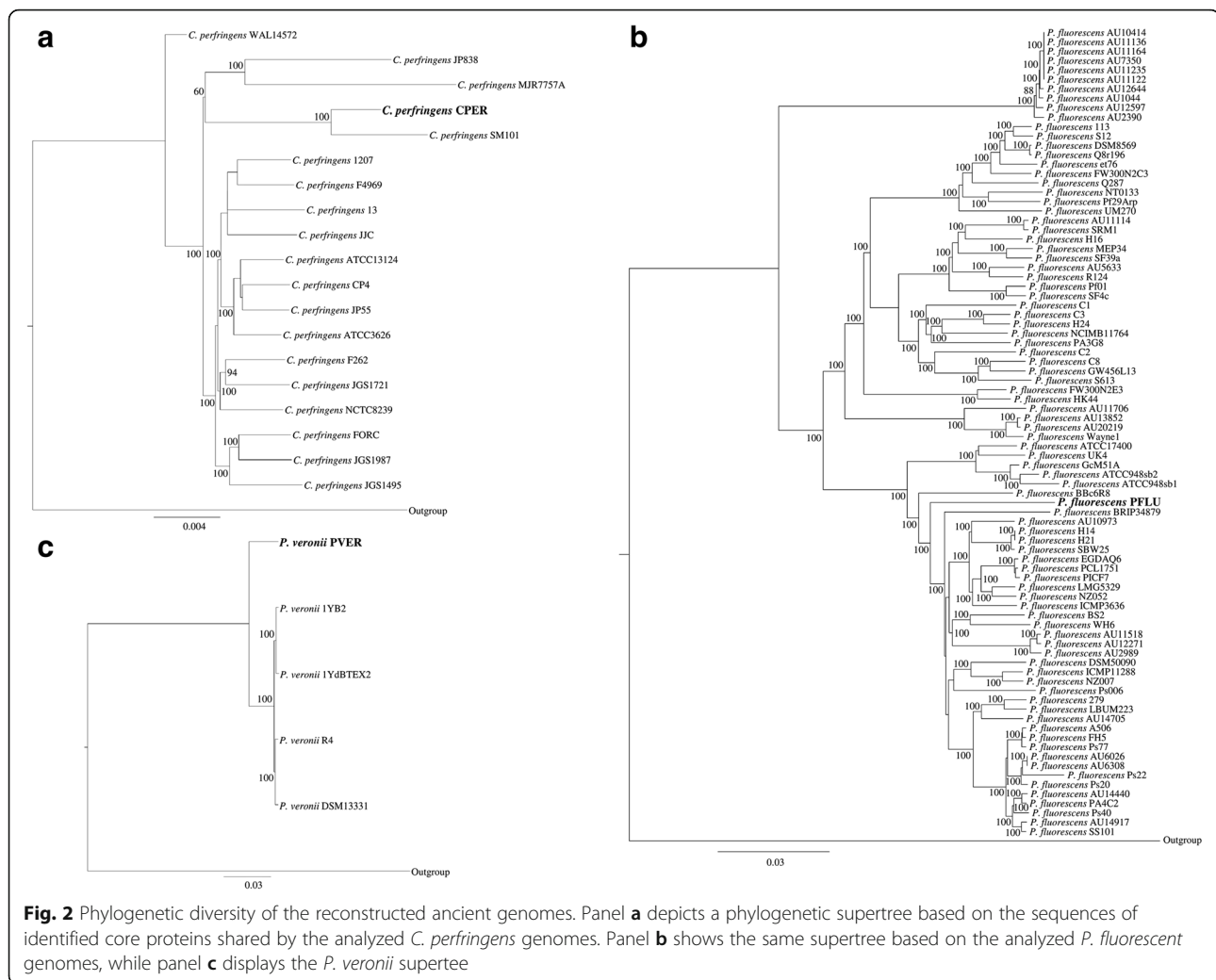


Fig. 2 Phylogenetic diversity of the reconstructed ancient genomes. Panel **a** depicts a phylogenetic supertree based on the sequences of identified core proteins shared by the analyzed *C. perfringens* genomes. Panel **b** shows the same supertree based on the analyzed *P. fluorescens* genomes, while panel **c** displays the *P. veronii* supertree

BLASTp homology search (cutoff E value of 1×10^{-30}) using the NCBI database. Notably, 68.4% of the truly unique genes (TUGs) of *C. perfringens* CPER appear to be unrelated to any genes belonging to members of this genus and 66.7% of these TUGs fail to share homology with any known protein sequence (Additional file 6: Figure S5 and Additional file 1: Table S5). Similarly, it was not possible to identify known homologs in the NCBI database for 47.8% of the TUGs identified in *P. veronii* PVER, suggesting that these TUGs may have been acquired by HGT or have been lost by modern strains.

Focusing on the virulence genes defined in the VF database, it was possible to predict their acquisition and/or loss during the evolution of the analyzed species with at least four available genomes, based on the phylogeny reconstructed by the core gene-based supertrees (Additional file 6: Figure S5). This analysis showed that a large majority (98.1%) of the virulence factors

of the *C. perfringens* pan-genome appears to have been acquired early by a species ancestor, thus being shared by all currently known *C. perfringens* strains (Additional file 6: Figure S5). Gene gain/loss reconstruction during evolution of *P. veronii* PVER suggests that this strain possesses 8% less virulence genes compared to the average of modern strains of the same species. This suggests that over the last 3500 years acquisition of virulence genes factors was one of the main evolutionary drivers for this taxon (Additional file 6: Figure S5).

Ancient unique genomic regions of Ötzi's microbiome

The Pan-genome predictions allowed the identification of TUGs representing Unique Genomic Regions (UGRs) belonging to the reconstructed genomes of the gut microbiota members harbored by the Tyrolean Iceman (Table 1 and Additional file 1: Table S5). The comparisons of *Clostridium* sp. CADE and *C. aldicarnis* CALG

with the publicly available genomic sequences of modern relatives revealed 215 and 216 TUGs, respectively, while *C. perfringens* CPER exhibits a higher number of TUGs among the ancient *Clostridium* species (i.e., 493) (Table 1). Moreover, *P. veronii* PVER appears to contain a higher number of unique genes, i.e., 615 TUGs, which is probably a reflection of its larger genome size.

Genome comparisons between the chromosome sequence of *Clostridium* sp. Ade.TY and those of modern relatives revealed the absence of a major region (Fig. 3 and Additional file 7: Figure S6), which contains a gene cluster predicted to encode a β -D-glucuronide and D-glucuronate degradation super-pathway and a smaller region with a complete phosphotransferase system (PTS),

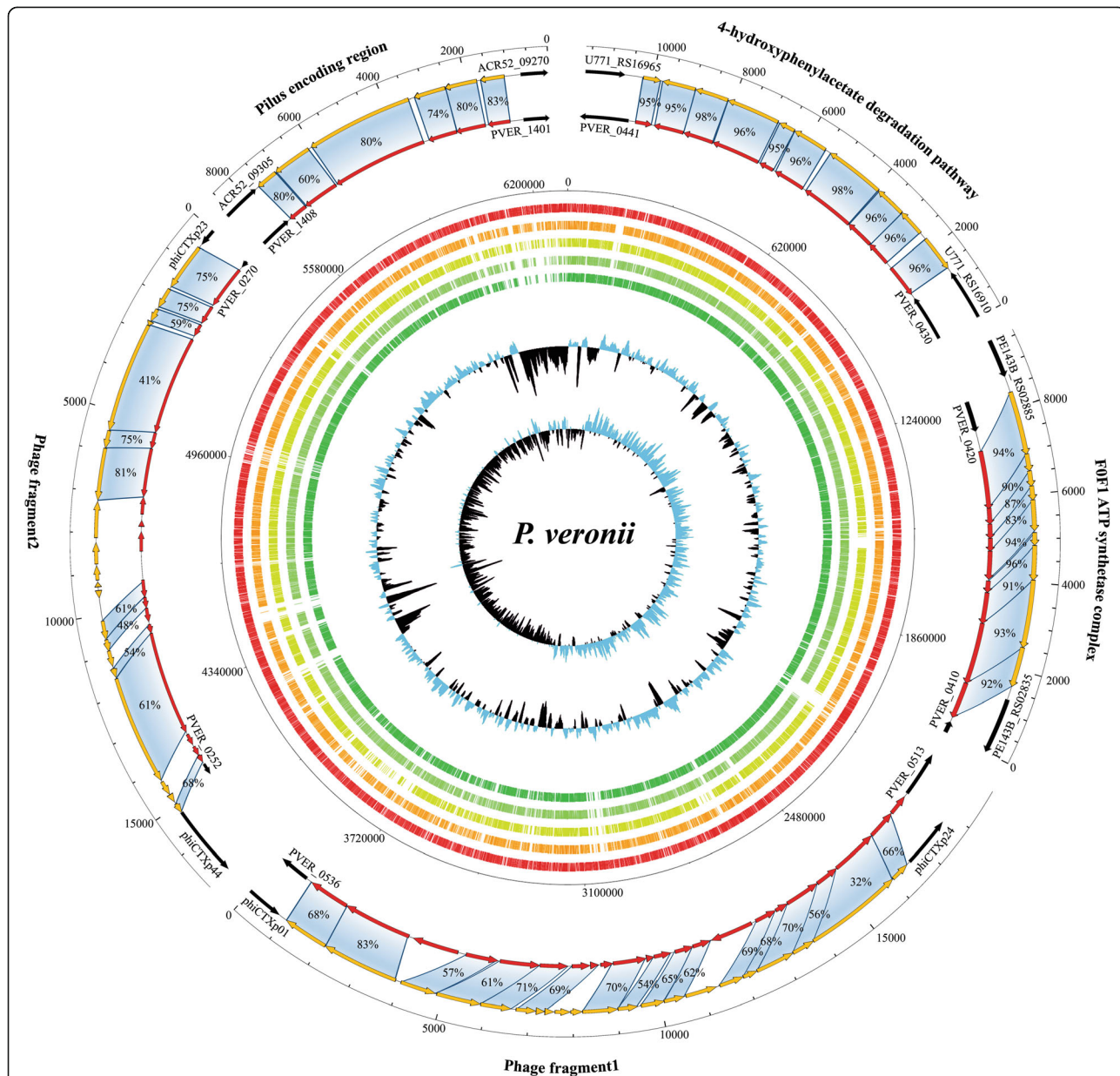


Fig. 3 Comparative genomic analysis of *P. veronii* PVER with other fully sequenced *P. veronii* strains. Circular genome atlas of *P. veronii* PVER (red circle) with mapped orthologues (defined as reciprocal best BLASTp hits with more than 50% identity over at least 50% of both protein lengths) in four publicly available *P. veronii* genomes (orange through green circle). Internal circles illustrate *P. veronii* PVER GC% deviation and GC skew (G – C/G + C), while the external maps exhibit the sequence identity between the unique loci of *P. veronii* PVER compared to other bacteria retrieved from the database. Each arrow indicates an ORF, whereas the length of the arrow is proportional to the length of the predicted ORF. Red arrows correspond to the *P. veronii* PVER genes, while orange arrows display orthologous genes

Table 2 *Clostridium perfringens* toxins

CPER ORFs	VFDB subject	Identity	Al- len	Mismatch	Gap openings	Q.start	Q.end	S.start	S.end	log (e value)	Bit score	Predicted annotation
CPER_0621	VFG002284 (gi:18309535) (nanJ) exo-alpha-sialidase [sialidase (VF0391)] [<i>Clostridium perfringens</i> str. 13]	94.4	1173	66	0	1	1173	1	1173	-10000	2225.7	Exo-alpha-sialidase
CPER_0726	VFG002274 (gi:18309018) (plc) phospholipase C [alpha-toxin (CpPLC) (VF0378)] [<i>Clostridium</i> <i>perfringens</i> str. 13]	98.2	398	7	0	1	398	1	398	-240.2	826.2	Phospholipase C
CPER_0764	VFG002279 (gi:18310216) (nagJ) hyaluronidase [mu- toxin (VF0389)] [<i>Clostridium</i> <i>perfringens</i> str. 13]	98.1	879	17	0	1	879	1	879	-10000	1726.1	Hyaluronidase
CPER_1090	VFG002276 (gi:18309155) (colA) collagenase [kappa- toxin (VF0388)] [<i>Clostridium</i> <i>perfringens</i> str. 13]	98.3	1043	18	0	1	1043	62	1104	-10000	2096.2	Peptidase M9
CPER_1851	VFG002278 (gi:18309863) (nagI) hyaluronidase [mu- toxin (VF0389)] [<i>Clostridium</i> <i>perfringens</i> str. 13]	98.6	1297	18	0	1	1297	1	1297	-10000	2558.1	Hyaluronidase
CPER_2203	VFG002282 (gi:18309828) (cloSI) alpha-clostripain [alpha-clostripain (VF0390)] [<i>Clostridium</i> <i>perfringens</i> str. 13]	97.3	522	14	0	1	522	3	524	-304.5	1040	Alpha-clostripain precursor
CPER_2247	VFG002280 (gi:18310261) (nagK) hyaluronidase [mu- toxin (VF0389)] [<i>Clostridium</i> <i>perfringens</i> str. 13]	99.3	1157	8	0	1	1157	1	1157	-10000	2315.8	Hyaluronidase
CPER_2490	VFG002285 (gi:110800384) (nanH) sialidase [sialidase (VF0391)] [<i>Clostridium</i> <i>perfringens</i> ATCC 13124]	95.9	294	12	0	1	294	89	382	-168.5	587.4	Exo-alpha-sialidase
CPER_2569	VFG002277 (gi:18309173) (nagH) hyaluronidase [mu- toxin (VF0389)] [<i>Clostridium</i> <i>perfringens</i> str. 13]	98	1058	21	0	1	1058	21	1078	-10000	2120.1	Hyaluronoglucosaminidase
CPER_2658	VFG002283 (gi:18309707) (nanI) exo-alpha-sialidase [sialidase (VF0391)] [<i>Clostridium</i> <i>perfringens</i> str. 13]	99.7	694	2	0	1	694	1	694	-10000	1404.4	Exo-alpha-sialidase

Table 2 *Clostridium perfringens* toxins (Continued)

CPER_2774	VFG002281 (gi:18310505) (nagL) hyaluronidase [mu- toxin (VF0389)] [<i>Clostridium</i> <i>perfringens</i> str. 13]	97.9	900	19	0	9	908	1	900	-10000	1787.3	Hyaluronidase
CPER_2934	VFG002275 (gi:18309145) (pfoA) perfringolysin O [theta-toxin/PFO (VF0382)] [<i>Clostridium</i> <i>perfringens</i> str. 13]	99.8	500	1	0	1	500	1	500	-289.6	990.7	Perfringolysin O

highlighting additional capability in the uptake of carbohydrates and energy production. In contrast, *C. algidicarnis* CALG possesses (compared to the genome of *C. algidicarnis* B3) many unique, yet small genomic regions scattered with genes coding for hypothetical proteins. Notably, one of these unique *C. algidicarnis* CALG regions encompasses a complete type III restriction modification system (RM system), which is absent in the modern strain. The *C. perfringens* CPER atlas analysis showed that the genome of *C. perfringens* str. 13 possesses a very simplified genome, while the other 16 publicly available strains analyzed showed the widespread presence of unique genomic regions that all appear to be present in the reference genome of *C. perfringens* CPER. These data suggest that *C. perfringens* CPER probably represents an ancestral genome with higher genetic complexity than the modern *C. perfringens* strains, which seems to have undergone an innovation phase that was aimed at increasing genome complexity without following a reductive phase to achieve genome simplification by gene loss.

Interestingly, the genome of *P. veronii* PVER, when aligned with the four chromosome sequences of contemporary *P. veronii* strains, shows many unique genomic regions, rendering this genome one of the most interesting ancient bacterial genomes in terms of identified unique genes. Remarkably, the most characteristic unique loci were shown to include a prophage, a FOF1 ATP synthetase complex, a 4-hydroxyphenylacetate degradation pathway and a pilus-encoding region (Fig. 3). Notably, a comparison of the *P. veronii* PVER prophage's unique gene content reveals extensive homology with phage CTX isolated from *Pseudomonas aeruginosa* [59]. More than half of the total ORFeome of the identified prophage (29) displays a marked homology (from 43.1 to 83.4%) to ϕ CTX genes (Fig. 3). The unique pilus-encoding genes show high sequence identity (from 59.5 to 83.4%) to homologs located on the genome of *Pseudomonas* sp. KG01, isolated from the Antarctic (Fig. 3). Interestingly, the publicly available *P. veronii* strains were isolated

from soil and water samples [58]; thus, we can assume that the ancient *P. veronii* PVER may have possessed peculiar systems that assisted this strain in human gut colonization. Accordingly, the modern *P. veronii* strains may have lost the pilus-encoding capacity, perhaps together with its capability to colonize the human gut. Furthermore, the unique FOF1 complex identified in *P. veronii* PVER shares high sequence identity to the same complex of *Pseudomonas extremaustralis* strain 14-3 (from 84.3 to 95.8%) (Fig. 3), a bacterium isolated from a temporary pond in Antarctica. Interestingly, the phylogenetic relatedness between *P. extremaustralis* strain 14-3 and other *P. veronii* strains had been described previously [60].

Toxin-encoding genes and antibiotic resistance in the ancient Ötzi strains

Since members of the *Clostridium* genus produce a wide range of toxins and secreted virulence factors [61], the toxin and virulence factor-encoding genes are intensively exploited as a key typing system for *C. perfringens*. This species is one of the most prolific producers of toxins [62], with five biotypes (A–E) delineated on the basis of the differential production of α , β , ϵ , and ι toxins [55]. Using a custom database composed of toxin sequences of well-known *C. perfringens* strains, we were able to predict the toxins that may be synthesized by *C. perfringens* CPER. Specifically, the prehistoric *C. perfringens* CPER was predicted to encode the α -toxin (phospholipase C) associated with the biotype A of *C. perfringens* species (99.2% sequence identity compared to that encoded by the NRRL B-23841 strain) (Table 2). Interestingly, in humans, biotype A is typically associated with food poisoning [55]. Furthermore, thanks to the virulence factor and NCBI databases, we were able to identify other *C. perfringens* toxins in the reconstructed ancient genome that are currently not used as biotype delineators, such as β 2-toxin (CPB2), θ -toxin (perfringolysin O), μ -toxin (hyaluronidase), κ -toxin (collagenase), and several enterotoxins (CPE) (Table 2). Notably, β 2-toxin is associated with

Table 3 Predicted toxin-antitoxin systems

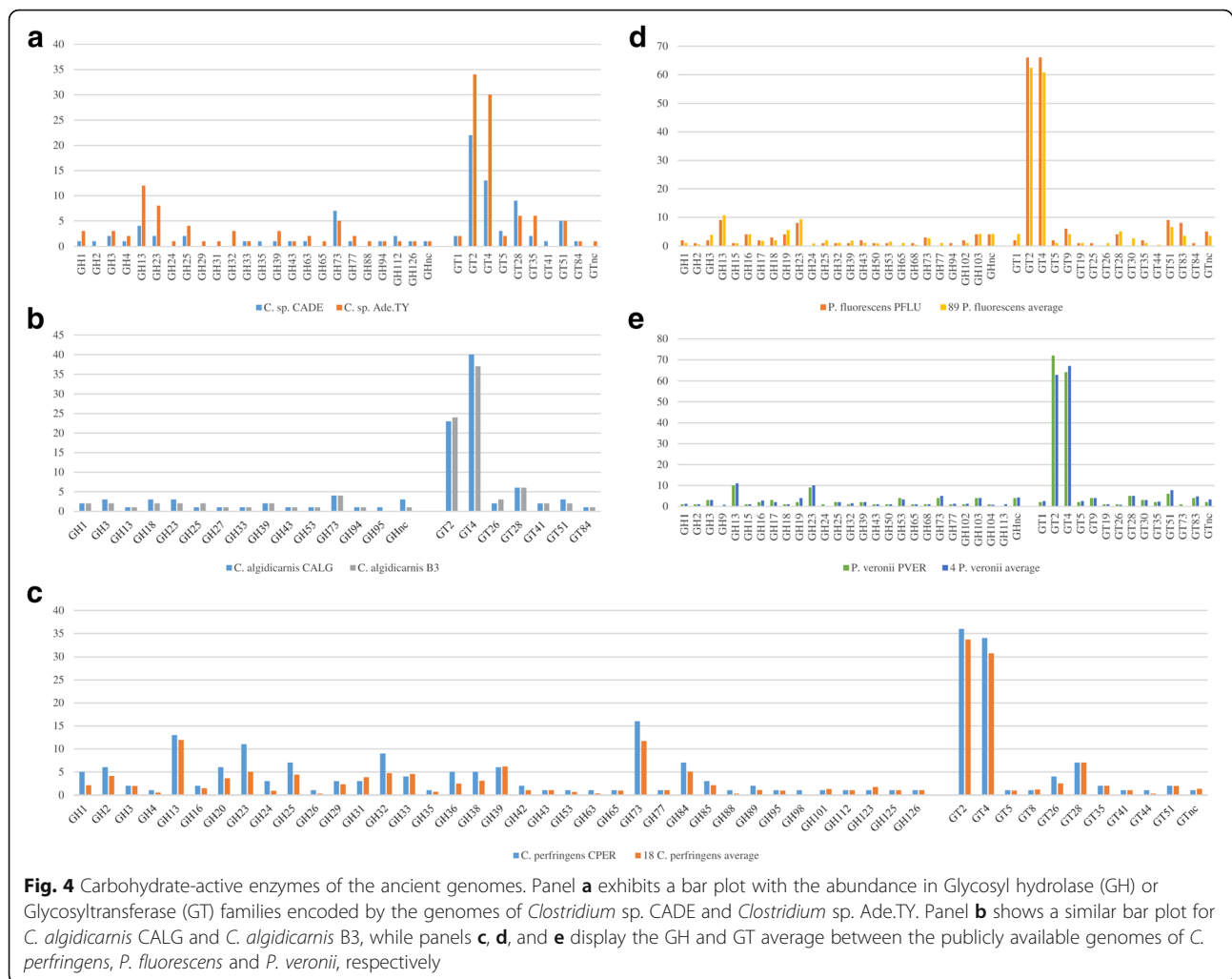
Ancient ORFs	TADB code	TADB gene	Subject	Identity	Aln-len	Mismatch	Gap openings	Q.start	Q.end	S.start	S.end	Log (e value)	Bit score	Predicted annotation
CADE_0165	TADB 8353403	CLL_A3362	<i>Clostridium botulinum</i> B str. Eklund 17B	96.6	116	4	0	1	116	1	116	-57.5	216.9	mRNA interferase PemK
CADE_0166	-	-	-	-	-	-	-	-	-	-	-	-	-	Hypothetical protein
CALG_0512	TADB 8436183	CLH_2005	<i>Clostridium botulinum</i> E3 str. Alaska E43	76.7	146	34	0	1	146	1	146	-64.3	240	Hypothetical protein
CALG_0513	TADB 8436181	CLH_2004	<i>Clostridium botulinum</i> E3 str. Alaska E43	63.8	127	46	0	4	130	6	132	-45.3	176.4	Hypothetical protein
CALG_1265	TADB 375739	CAC0494	<i>Clostridium acetobutylicum</i> ATCC 824	90.4	114	11	0	3	116	2	115	-54.3	206.5	mRNA interferase PemK
CALG_1266	-	-	-	-	-	-	-	-	-	-	-	-	-	CopG family transcriptional regulator
CPER_1456	TADB 4710268	CPF_0812	<i>Clostridium perfringens</i> ATCC 13124	95.8	71	3	0	1	71	1	71	-35.6	144.4	Hypothetical protein
CPER_1457	TADB 607725	CPE0814	<i>Clostridium perfringens</i> str. 13	97.5	162	4	0	1	162	1	162	-87.9	318.2	GNAT family acetyltransferase
CPER_2012	TADB 4710831	CPF_1033	<i>Clostridium perfringens</i> ATCC 13124	99.4	168	1	0	1	168	1	168	-95.5	343.6	Hypothetical protein
CPER_2013	TADB 4710829	CPF_1032	<i>Clostridium perfringens</i> ATCC 13124	100	69	0	0	1	69	1	69	-34	139	DNA-binding protein
CPER_2208	TADB 4721113	CPR_0896	<i>Clostridium perfringens</i> SM101	97.2	143	4	0	1	143	1	143	-77.7	284.3	Hypothetical protein
CPER_3173	TADB 4710797	CPF_1020	<i>Clostridium perfringens</i> ATCC 13124	97.9	140	3	0	7	146	1	140	-75.2	275.8	Hypothetical protein
CPER_3174	TADB 4710799	CPF_1021	<i>Clostridium perfringens</i> ATCC 13124	95.6	180	8	0	1	180	1	180	-93.5	337	XRE family transcriptional regulator
PFLU_1561	TADB 9079447	PFLU2030	<i>Pseudomonas fluorescens</i> SBW25	98.4	123	2	0	1	123	1	123	-64.8	241.1	Hypothetical protein
PFLU_1562	TADB 9079443	PFLU2029	<i>Pseudomonas fluorescens</i> SBW25	88.5	113	12	1	1	112	1	113	-50.8	194.9	Cro/C1 family transcriptional regulator
PFLU_2731	-	-	-	-	-	-	-	-	-	-	-	-	-	Hexulose-6-phosphate isomerase
PFLU_2732	TADB 348443	hicB-2	<i>Pseudomonas putida</i> KT2440	71.3	108	31	0	5	112	2	109	-42.4	166.8	Antitoxin HicB
PFLU_4077	-	-	-	-	-	-	-	-	-	-	-	-	-	Protein RnfH
PFLU_4078	-	-	-	-	-	-	-	-	-	-	-	-	-	Ribosome association toxin RatA
PVER_0551	TADB 12012688	BCAS0580	<i>Burkholderia cenocepacia</i> J2315	55.8	129	56	1	1	128	1	129	-35.9	145.2	Twitching motility protein P1IT

Table 4 Ancient metabolic pathways

Species	Pathways	Status	Enzymes	Genes	Starting molecule	Final product						
<i>Clostridium</i> sp. CADE	PreQ0 biosynthesis	Complete	GTP cyclohydrolase I	<i>folE</i>	guanosine 5'-triphosphate (GTP)	7-cyano-7- deazaguanine (preQ0)						
			6-carboxy-5,6,7, 8-tetrahydropterin synthase	<i>queD</i>								
			7-carboxy-7- deazaguanine synthase	<i>queE</i>								
		7-cyano-7-deazaguanine synthase		<i>queC</i>								
	β -D-glucuronide and D-glucuronate degradation	Complete	β -D-glucuronidase	<i>uidA</i>	β -D-glucuronoside	D-fructuronate						
			D-glucuronate isomerase	<i>uxaC</i>								
			D-mannonate oxidoreductase	<i>uxuB</i>								
			D-mannonate dehydratase	<i>uxuA</i>								
			2-keto-3- deoxygluconokinase	<i>kdgK</i>								
			2-keto-3-deoxygluconate 6-phosphate aldolase	<i>eda</i>								
Flavin biosynthesis I	Partial	bifunctional riboflavin kinase/FMN adenyltransferase	<i>ribF</i>	Guanosine 5'-triphosphate (GTP)	Flavin adenine dinucleotide (FAD)							
		5-amino-6-(5-phospho- D- ribitylamino) uracil phosphatase	<i>ybjI</i>									
		3,4-dihydroxy-2-butanone 4-phosphate synthase	<i>ribB</i>									
	Biotin biosynthesis from 8-amino-7-oxononanoate I	Partial	Biotin synthase	<i>bioB</i>	8-amino-7- oxononanoate (KAPA)	Vitamin H (biotin)						
							Biotin biosynthesis from 8-amino-7-oxononanoate II	Partial	Biotin synthase	<i>bioB</i>	8-amino-7- oxononanoate (KAPA)	Vitamin H (biotin)
<i>C. algidicarnis</i> CALG	Myo-, chiro- and scillo- inositol degradation	Partial	(methyl) malonate- semialdehyde dehydrogenase gene	<i>mmsA</i>	Inositol	Glycerone phosphate (DHAP) + acetyl-CoA						
							Myo-inositol degradation	Partial	(methyl) malonate- semialdehyde dehydrogenase gene	<i>mmsA</i>	Inositol	Glycerone phosphate (DHAP) + acetyl-CoA
<i>P. fluorescens</i> PFLU	KDO transfer to lipid IVA I	Absent	–	–	CMP-3-deoxy- β -D-manno- octulosonate	α -Kdo-(2- > 4)- α -Kdo- (2- > 6)-lipid IVA						
							KDO transfer to lipid IVA II	Absent	–	–	CMP-3-deoxy- β -D- manno-octulosonate	4-O-phospho- α -Kdo- (2 \rightarrow 6)-lipid IVA
<i>P. veronii</i> PVER	Pyochelin biosynthesis	Absent	–	–	L-cysteine	Pyochelin						
							4-hydroxyphenylacetate degradation	Complete	4-coumarate 3-monooxygenase	<i>hpaB</i>	4-hydroxyphenylacetate	Succinate

enteritis in animals [63], while θ -toxin can damage blood vessels, resulting in leukostasis, thrombosis, and tissue hypoxia. More interestingly, the high number of enterotoxins indicates a high probability that *C. perfringens*

CPER was able to cause (symptoms of) food poisoning, as also suggested by the fact that modern CPE-producing type A strains are major human gut pathogens [64]. However, the reconstructed genome of *C. perfringens* CPER



strain does not include those toxins that can ultimately lead to death in humans (β and ϵ toxins), indicating that this particular pathogenic characteristic may have been introduced in the modern strains in order to increase the ecological fitness of the *C. perfringens* species.

Moreover, the prediction of toxin-antitoxin systems (TA) was performed for the complete reconstructed genomes, in order to explore the capabilities of these strains to control cell growth and bacterial persistence. The generated information revealed the presence of a small number of complete TA systems in the *Clostridium* genomes, ranging from one in *Clostridium* sp. CADE to three in *C. perfringens* CPER, and an extraordinary richness of 11 such systems in the *P. veronii* PVER chromosome (Table 3). Recently, a high abundance in TA systems has been correlated with pathogenicity of epidemic bacteria such as *Mycobacterium tuberculosis* [65], while TA systems are more abundant in free-living microorganisms rather than host-associated

species [66]. Thus, *P. veronii* PVER does not seem to possess a distinguishing TA system-associated profile of host-associated commensals, but, rather, a profile that is reminiscent of highly pathogenic bacteria adapted to survive and persist in their environment.

Additionally, an antibiotic resistance (AR) gene profiling was conducted on the identified genes of the ancient Ötzi's strains and the related publicly available genomes. The screening highlighted abundance in putative beta-lactamase and glycopeptide resistance proteins as well as various transporters belonging to the ATP-binding cassette (ABC) uptake porters and major facilitator superfamily (MFS). Interestingly, modern strains appear to possess a larger arsenal of AR-encoding genes. In particular, modern *P. veronii* and *Clostridium* genomes show 24% and up to 17% more AR genes compared to their ancient relatives *P. veronii* PVER and *C. algidicarnis* CALG, respectively. Such observations reveal that the genomes of modern strains have developed or

horizontally acquired a larger AR-encoding gene arsenal, perhaps in order to counteract the introduction of antibiotics in the modern era.

Functional profiling of prehistoric microbial genomes

A functional profiling as well as an enzymatic gene classification was performed to evaluate the metabolic pathways encoded by the reconstructed prehistoric genomes. This *in silico* metabolic profiling showed that the ancient strains encode various complete pathways that appear to be absent in modern strains, e.g., the “preQ0 biosynthesis” of *Clostridium* sp. CADE, as well as absence of complete pathways identified in the modern strains, e.g., the “myo-, chiro-, and scillo-inositol degradation” in *C. algidicarnis* CALG and the “pyochelin biosynthesis” in *P. veronii* PVER (Table 4). Interestingly, *Clostridium* sp. CADE lacks the “sucrose degradation I (sucrose phosphotransferase)” pathway, as well as alternative sucrose degradation pathways, indicating that the ancient strain was not able to use sucrose in order to produce β -D-glucose 6-phosphate and β -D-fructofuranose 6-phosphate as glycolytic substrates. In contrast, as shown from the unique loci analysis, a complete pathway for the “ β -D-glucuronide and D-glucuronate degradation” was detected, highlighting the capability to produce D-fructuronate, which may then be further degraded into D-glyceraldehyde 3-phosphate and pyruvate (Table 4). Another intriguing finding with respect to the differences in metabolic capabilities between prehistoric vs. contemporary strains is represented by the ability to degrade 4-hydroxyphenylacetate. *P. veronii* PVER, as discussed before, shows a complete 4-hydroxyphenylacetate degradation pathway already identified in other strains belonging to the Proteobacteria phylum, highlighting the capability to produce succinate and pyruvate from alternative carbon sources (Table 4).

Investigation of the Carbohydrate Active Enzymes using the CAZY database [48] highlighted intriguing differences between modern and ancient genomes, which may explain a specific adaptation of the modern strains to novel ecological niches. It was noted that the genome of *C. sp.* CADE possesses a lower abundance in Glycosyl Hydrolases (GHs) and Glycosyl Transferases (GTs) compared to the *Clostridium* sp. Ade.TY strain, exhibiting a reduction in genes that encode such enzymes by 46.6 and 33.3%, respectively (Fig. 4). This smaller GH arsenal is in particular due to reduced numbers of members of GH13 and GH23 families, which are predicted to be involved in the hydrolysis of substrates containing α -glucoside linkages such as maltose. In contrast, the genome of *C. perfringens* CPER shows a higher abundance in GHs (28.6%) and GTs (8%) compared to the average of the 18 sequenced modern strains (Fig. 4). A substantial proportion of these GHs belong to the GH23 and GH32 families, highlighting an improved capability for the hydrolysis of fructose-containing

sugars compared to the other 18 *C. perfringens* strains. In contrast, the predicted GH and GT repertoire of the *P. veronii* PVER genome, when compared to that of modern strains, revealed a similar composition in its carbohydrate-active enzyme profile (Fig. 4).

Conclusions

Next generation sequencing (NGS) approaches are a valuable resource allowing the exploration of the composition and functionalities of the human gut microbiota in the soft tissue of human mummies. In this study, we performed an *in depth* metagenomic analysis of four biopsy samples recently retrieved from the small and large intestines of the Tyrolean Iceman [21], resulting in the reconstruction and characterization of ancient microbial genomes that were predominant in the Tyrolean Iceman’s distal gut at death. The reconstructed genomes of *C. perfringens*, *Clostridium* sp. Ade.TY, *C. algidicarnis*, and *P. veronii* allowed the identification of evolutionary development of these taxa. The reconstructed genome of *Clostridium* sp. CADE displayed high genomic variability with the chromosome of the related *Clostridium* sp. Ade.TY; thus, it may be considered as a novel *Clostridium* species that is capable of degrading glucuronate, yet is unable to metabolize sucrose. Interestingly, analyses performed on the ancient genome *C. perfringens* CPER highlight a similar genome structure and a phylogenetic relatedness with the enterotoxin-producing food poisoning strain *C. perfringens* SM101. Furthermore, the identification of genes that encode the α -toxin (phospholipase C) and various other enterotoxins suggest that *C. perfringens* CPER was a human food poisoning strain associated with the biotype A of toxigenic *C. perfringens* species. Despite the fact that modern *P. veronii* strains have been isolated from water springs, the ancient strain PVER seems to possess the ability to colonize the human gut (pre- or post-mortem). Moreover, *P. veronii* PVER is related to *Pseudomonas* strains isolated from the Antarctic, thus supporting its ancient origin. Notably, gene gain/loss prediction showed that one of the main forces driving the evolution of *P. veronii* was the development and/or acquisition of novel virulence factors. While modern/ancient average ratio of the predicted antibiotic resistances suggests that the modern strains have been subjected to substantial selective pressure, possibly due to the extensive use of antibiotics in the modern era.

Additional files

Additional file 1: Tables S1, S2, S3, S4, and S5.

Additional file 2: Figure S1. Bacterial abundance in Ötzi’s gut. Panel a displays a bar plot with the abundance of the major species identified in the Tyrolean Iceman gut using MEGAN5 software. The x axis represents the identified bacterial species, while the y axis represents the number of reads. Each color reflects a specific sample, i.e., B0625 (lower part of the

large intestine), C1824 and C1825 (upper part of the large intestine), and B0621 (small intestine). Panel b visually displays the observed abundance of the identified species.

Additional file 3: Figure S2. Cytosine to thymine substitution frequency at the 5' end of the sequenced reads. The plot displays the cytosine deamination pattern of the *Clostridium* sp. CADE, *C. algidicarnis* CALG, *C. perfringens* CPER, *P. fluorescens* PFLU, and *P. veronii* PVER selected reads from the Ötzi's metagenomic samples. The y axis reports the C to T substitution frequency, while the x axis indicates the distance from the 5' end of the sequence reads.

Additional file 4: Figure S3. Mauve alignment of reconstructed ancient *H. pylori* to the reference *H. pylori* 26695. On top the reference *H. pylori* 26695 genome is depicted, while the reordered contigs of the reconstructed ancient *H. pylori* from the Ötzi's metagenomics samples is indicated on the bottom part of the figure. Each colored block corresponds to a conserved genomic region between the two genome sequences, while the red line discerns the ancient *H. pylori* contigs.

Additional file 5: Figure S4. CG content/coverage plot of ancient reconstructed genome contigs. Panel a displays the CG content distribution of the *Clostridium* sp. CADE contigs; similarly, panels b to d display this for *C. algidicarnis* CALG, *C. perfringens* CPER, and *P. veronii* PVER contigs, respectively.

Additional file 6: Figure S5. Evolutionary gain and loss analysis based on predicted virulence factors within *C. perfringens*, *P. fluorescens*, and *P. veronii* species. Panel a displays the core gene-based supertree of *C. perfringens* strains, where each node reports the number of predicted virulence factor COGs identified for each strain. Furthermore, gains and losses are indicated by green and orange bars on the edge leading to each node. Panels b and c show the same analysis conducted on *P. fluorescens* and *P. veronii* species, respectively.

Additional file 7: Figure S6. Comparative genomic analysis of *Clostridium* sp. CADE, *C. algidicarnis* CALG, and *C. perfringens* CPER with other fully sequenced strains. Panel a displays the circular genome atlas of *Clostridium* sp. CADE (red circle) with mapped orthologues (defined as reciprocal best BLASTp hits with more than 50% identity over at least 50% of both protein lengths) in public available *Clostridium* sp. Ade.TY genome (orange circle). Internal circles illustrate GC% deviation and GC skew ($G - C/G + C$). Panel b and c shows the same circular genome atlas of *C. algidicarnis* CALG and *C. perfringens* CPER, respectively.

Abbreviations

ABC: ATP-binding cassette; ANI: Average nucleotide identity; AR: Antibiotic resistance; COG: Clusters of orthologous genes; CPE: *Clostridium perfringens* enterotoxins; GF: Gene family; GH: Glycosyl hydrolases; GT: Glycosyltransferases; HGT: Horizontal gene transfer; HMM: Hidden Markov model; MFS: Major facilitator superfamily; NCBI: National Center for Biotechnology Information; NGS: Next-generation sequencing; ORF: Open reading frames; PTS: Phosphotransferase system; TA: Toxin-antitoxin systems; TUG: Truly unique genes; UGR: Unique genomic regions

Acknowledgements

We gratefully acknowledge Frank Maixner and Albert Zink (Institute for Mummies and the Iceman, European Academy of Bozen/Bolzano (EURAC), Viale Druso 1, 39100 Bolzano, Italy.) for having shared their metagenomic data with us and Thomas Rattei (CUBE-Division of Computational Systems Biology, Department of Microbiology and Ecosystem Science, University of Vienna, Althanstrasse 14, 1090 Vienna, Austria) for the help in collecting those data.

Funding

We thank GenProbio srl for the financial support of the Laboratory of Probiogenomics. DvS is a member of the APC Microbiome Institute funded by Science Foundation Ireland (SFI), through the Irish Government's National Development Plan (Grant number SFI/12/RC/2273).

Availability of data and materials

The sequence data supporting the results of this article are available in the European Nucleotide Archive under accession ERP012908.

Authors' contributions

GAL processed the metagenomic data, generated the custom script CoCla, conducted the analysis, and wrote the manuscript. CM participated in the design of the study and contributed to the manuscript preparation. LM contributed to generate the custom script CoCla. FT, CF, and SD participated in the design of the study. DvS participated and supervised the study. MV conceived the study, participated in its design and coordination, and contributed to the manuscript preparation. All authors read and approved the final manuscript.

Competing interests

The authors declare that they have no competing interests.

Ethics approval and consent to participate

Not applicable.

Consent for publication

Not applicable.

Author details

¹Laboratory of Probiogenomics, Department of Life Sciences, University of Parma, Parco Area delle Scienze 11a, 43124 Parma, Italy. ²APC Microbiome Institute and School of Microbiology, National University of Ireland, Cork, Ireland.

Received: 5 July 2016 Accepted: 13 December 2016

Published online: 17 January 2017

References

- Gill SR, Pop M, Deboy RT, Eckburg PB, Turnbaugh PJ, Samuel BS, Gordon JL, Relman DA, Fraser-Liggett CM, Nelson KE. Metagenomic analysis of the human distal gut microbiome. *Science*. 2006;312:1355–9.
- Kurokawa K, Itoh T, Kuwahara T, Oshima K, Toh H, Toyoda A, Takami H, Morita H, Sharma VK, Srivastava TP, et al. Comparative metagenomics revealed commonly enriched gene sets in human gut microbiomes. *DNA Res*. 2007;14:169–81.
- Kamada N, Chen GY, Inohara N, Nunez G. Control of pathogens and pathobionts by the gut microbiota. *Nat Immunol*. 2013;14:685–90.
- Milani C, Ticinesi A, Gerritsen J, Nouvenne A, Lugli GA, Mancabelli L, Turrioni F, Duranti S, Mangifesta M, Viappiani A, et al. Gut microbiota composition and *Clostridium difficile* infection in hospitalized elderly individuals: a metagenomic study. *Sci Rep*. 2016;6:25945.
- Gosalbes MJ, Abellan JJ, Durban A, Perez-Cobas AE, Latorre A, Moya A. Metagenomics of human microbiome: beyond 16 s rDNA. *Clin Microbiol Infect*. 2012;18 Suppl 4:47–9.
- Milani C, Hevia A, Foroni E, Duranti S, Turrioni F, Lugli GA, Sanchez B, Martin R, Gueimonde M, van Sinderen D, et al. Assessing the fecal microbiota: an optimized ion torrent 16S rRNA gene-based analysis protocol. *PLoS One*. 2013;8:e68739.
- Turrioni F, Marchesi JR, Foroni E, Gueimonde M, Shanahan F, Margolles A, van Sinderen D, Ventura M. Microbiomic analysis of the bifidobacterial population in the human distal gut. *ISME J*. 2009;3:745–51.
- Milani C, Mancabelli L, Lugli GA, Duranti S, Turrioni F, Ferrario C, Mangifesta M, Viappiani A, Ferretti P, Gorfer V, et al. Exploring vertical transmission of bifidobacteria from mother to child. *Appl Environ Microbiol*. 2015;81:7078–87.
- Ubaldi M, Luciani S, Marota I, Fornaciari G, Cano RJ, Rollo F. Sequence analysis of bacterial DNA in the colon of an Andean mummy. *Am J Phys Anthropol*. 1998;107:285–95.
- Cano RJ, Tiefenbrunner F, Ubaldi M, Del Cueto C, Luciani S, Cox T, Orkand P, Kunzel KH, Rollo F. Sequence analysis of bacterial DNA in the colon and stomach of the Tyrolean Iceman. *Am J Phys Anthropol*. 2000;112:297–309.
- Tito RY, Knights D, Metcalf J, Obregon-Tito AJ, Cleeland L, Najjar F, Roe B, Reinhard K, Sobolik K, Belknap S, et al. Insights from characterizing extinct human gut microbiomes. *PLoS One*. 2012;7:e51146.
- Cano RJ, Rivera-Perez J, Toranzos GA, Santiago-Rodriguez TM, Narganes-Storde YM, Chanlatte-Baik L, Garcia-Roldan E, Bunkley-Williams L, Massey SE. Paleomicrobiology: revealing fecal microbiomes of ancient indigenous cultures. *PLoS One*. 2014;9:e106833.

13. Warinner C, Rodrigues JF, Vyas R, Trachsel C, Shved N, Grossmann J, Radini A, Hancock Y, Tito RY, Fiddyment S, et al. Pathogens and host immunity in the ancient human oral cavity. *Nat Genet.* 2014;46:336–44.
14. Adler CJ, Dobney K, Weyrich LS, Kaidonis J, Walker AW, Haak W, Bradshaw CJ, Townsend G, Soltysiak A, Alt KW, et al. Sequencing ancient calcified dental plaque shows changes in oral microbiota with dietary shifts of the Neolithic and Industrial revolutions. *Nat Genet.* 2013;45:450–5. 455e451.
15. Morris JA, Harrison LM, Partridge SM. Postmortem bacteriology: a re-evaluation. *J Clin Pathol.* 2006;59:1–9.
16. Hofreiter M, Serre D, Poinar HN, Kuch M, Paabo S. Ancient DNA. *Nat Rev Genet.* 2001;2:353–9.
17. Lynnerup N. Mummies. *Am J Phys Anthropol.* 2007;134(S45):162–190.
18. Gip L, Aschan-Aberg K. Dermatophytes isolated from an open air public bath. *Acta Derm Venereol.* 1968;48:246–8.
19. Bos KI, Schuenemann VJ, Golding GB, Burbano HA, Waglechner N, Coombes BK, McPhee JB, DeWitte SN, Meyer M, Schmedes S, et al. A draft genome of *Yersinia pestis* from victims of the Black Death. *Nature.* 2011;478:506–10.
20. Schuenemann VJ, Singh P, Mendum TA, Krause-Kyora B, Jager G, Bos KI, Herbig A, Economou C, Benjak A, Busso P, et al. Genome-wide comparison of medieval and modern *Mycobacterium leprae*. *Science.* 2013;341:179–83.
21. Maixner F, Krause-Kyora B, Turaev D, Herbig A, Hoopmann MR, Hallows JL, Kusebauch U, Vigil EE, Malfertheiner P, Megraud F, et al. The 5300-year-old *Helicobacter pylori* genome of the Iceman. *Science.* 2016;351:162–5.
22. Williams AC, Edwards HG, Barry BW. The 'Iceman': molecular structure of 5200-year-old skin characterised by Raman spectroscopy and electron microscopy. *Biochim Biophys Acta.* 1995;1246:98–105.
23. Rollo F, Ubaldi M, Ermini L, Marota I. Otzi's last meals: DNA analysis of the intestinal content of the Neolithic glacier mummy from the Alps. *Proc Natl Acad Sci U S A.* 2002;99:12594–9.
24. Keller A, Graefen A, Ball M, Matzas M, Boisguerin V, Maixner F, Leidinger P, Backes C, Khairat R, Forster M, et al. New insights into the Tyrolean Iceman's origin and phenotype as inferred by whole-genome sequencing. *Nat Commun.* 2012;3:698.
25. Lazaridis I, Patterson N, Mittnik A, Renaud G, Mallick S, Kirsanow K, Sudmant PH, Schraiber JG, Castellano S, Lipson M, et al. Ancient human genomes suggest three ancestral populations for present-day Europeans. *Nature.* 2014;513:409–13.
26. Tang JN, Zeng ZG, Wang HN, Yang T, Zhang PJ, Li YL, Zhang AY, Fan WQ, Zhang Y, Yang X, et al. An effective method for isolation of DNA from pig faeces and comparison of five different methods. *J Microbiol Methods.* 2008;75:432–6.
27. Lee EJ, Makarewicz C, Renneberg R, Harder M, Krause-Kyora B, Muller S, Ostritz S, Fehren-Schmitz L, Schreiber S, Muller J, et al. Emerging genetic patterns of the European Neolithic: perspectives from a late Neolithic Bell Beaker burial site in Germany. *Am J Phys Anthropol.* 2012;148:571–9.
28. Kircher M, Sawyer S, Meyer M. Double indexing overcomes inaccuracies in multiplex sequencing on the Illumina platform. *Nucleic Acids Res.* 2012;40:e3.
29. Meyer M, Kircher M. Illumina sequencing library preparation for highly multiplexed target capture and sequencing. *Cold Spring Harb Protoc.* 2010; 2010:prot5448.
30. Lugli GA, Milani C, Mancabelli L, van Sinderen D, Ventura M. MEGAnnotator: a user-friendly pipeline for microbial genomes assembly and annotation. *FEMS Microbiol Lett.* 2016;363(7). doi:10.1093/femsle/fnw049. Epub 2016 Mar 1.
31. Bankevich A, Nurk S, Antipov D, Gurevich AA, Dvorkin M, Kulikov AS, Lesin VM, Nikolenko SI, Pham S, Prjibelski AD, et al. SPAdes: a new genome assembly algorithm and its applications to single-cell sequencing. *J Comput Biol.* 2012;19:455–77.
32. Ginolhac A, Rasmussen M, Gilbert MT, Willerslev E, Orlando L. mapDamage: testing for damage patterns in ancient DNA sequences. *Bioinformatics.* 2011;27:2153–5.
33. Darling AE, Mau B, Perna NT. progressiveMauve: multiple genome alignment with gene gain, loss and rearrangement. *PLoS One.* 2010;5:e11147.
34. Hyatt D, Chen GL, Locascio PF, Land ML, Larimer FW, Hauser LJ. Prodigal: prokaryotic gene recognition and translation initiation site identification. *BMC Bioinformatics.* 2010;11:119.
35. Zhao Y, Tang H, Ye Y. RAPSearch2: a fast and memory-efficient protein similarity search tool for next-generation sequencing data. *Bioinformatics.* 2012;28:125–6.
36. Lowe TM, Eddy SR. tRNAscan-SE: a program for improved detection of transfer RNA genes in genomic sequence. *Nucleic Acids Res.* 1997;25:955–64.
37. Lagesen K, Hallin P, Rodland EA, Staerfeldt HH, Rognes T, Ussery DW. RNAmmer: consistent and rapid annotation of ribosomal RNA genes. *Nucleic Acids Res.* 2007;35:3100–8.
38. Finn RD, Bateman A, Clements J, Coggill P, Eberhardt RY, Eddy SR, Heeger A, Hetherington K, Holm L, Mistry J, et al. Pfam: the protein families database. *Nucleic Acids Res.* 2014;42:D222–30.
39. Rutherford K, Parkhill J, Crook J, Horsnell T, Rice P, Rajandream MA, Barrell B. Artemis: sequence visualization and annotation. *Bioinformatics.* 2000;16:944–5.
40. Zhao Y, Wu J, Yang J, Sun S, Xiao J, Yu J. PGAP: pan-genomes analysis pipeline. *Bioinformatics.* 2012;28:416–8.
41. Enright AJ, Van Dongen S, Ouzounis CA. An efficient algorithm for large-scale detection of protein families. *Nucleic Acids Res.* 2002;30:1575–84.
42. Katoh K, Misawa K, Kumada K, Miyata T. MAFFT: a novel method for rapid multiple sequence alignment based on fast Fourier transform. *Nucleic Acids Res.* 2002;30:3059–66.
43. Larkin MA, Blackshields G, Brown NP, Chenna R, McGettigan PA, McWilliam H, Valentin F, Wallace IM, Wilm A, Lopez R, et al. Clustal W and Clustal X version 2.0. *Bioinformatics.* 2007;23:2947–8.
44. Richter M, Rossello-Mora R. Shifting the genomic gold standard for the prokaryotic species definition. *Proc Natl Acad Sci U S A.* 2009;106:19126–31.
45. Csuros M. Count: evolutionary analysis of phylogenetic profiles with parsimony and likelihood. *Bioinformatics.* 2010;26:1910–2.
46. Saier Jr MH, Reddy VS, Tamang DG, Vastermark A. The transporter classification database. *Nucleic Acids Res.* 2014;42:D251–8.
47. Chen L, Zheng D, Liu B, Yang J, Jin Q. VFDB 2016: hierarchical and refined dataset for big data analysis—10 years on. *Nucleic Acids Res.* 2016;44:D694–7.
48. Lombard V, Golaconda Ramulu H, Drula E, Coutinho PM, Henrissat B. The carbohydrate-active enzymes database (CAZY) in 2013. *Nucleic Acids Res.* 2014;42:D490–5.
49. Caspi R, Altman T, Billington R, Dreher K, Foerster H, Fulcher CA, Holland TA, Keseler IM, Kothari A, Kubo A, et al. The MetaCyc database of metabolic pathways and enzymes and the BioCyc collection of Pathway/Genome Databases. *Nucleic Acids Res.* 2014;42:D459–71.
50. Huson DH, Mitra S, Ruscheweyh HJ, Weber N, Schuster SC. Integrative analysis of environmental sequences using MEGAN4. *Genome Res.* 2011;21:1552–60.
51. Scales BS, Dickson RP, LiPuma JJ, Huffnagle GB. Microbiology, genomics, and clinical significance of the *Pseudomonas fluorescens* species complex, an unappreciated colonizer of humans. *Clin Microbiol Rev.* 2014;27:927–48.
52. Madi A, Alnabhani Z, Leneveu C, Mijouin L, Feuilloley M, Connil N. *Pseudomonas fluorescens* can induce and divert the human beta-defensin-2 secretion in intestinal epithelial cells to enhance its virulence. *Arch Microbiol.* 2013; 195:189–195.
53. Rizzi E, Lari M, Gigli E, De Bellis G, Caramelli D. Ancient DNA studies: new perspectives on old samples. *Genet Sel Evol.* 2012;44:21.
54. Konstantinidis KT, Tiedje JM. Genomic insights that advance the species definition for prokaryotes. *Proc Natl Acad Sci U S A.* 2005;102:2567–72.
55. Hassan KA, Elbourne LD, Tetu SG, Melville SB, Rood JJ, Paulsen IT. Genomic analyses of *Clostridium perfringens* isolates from five toxinotypes. *Res Microbiol.* 2015;166:255–63.
56. Scales BS, Erb-Downward JR, Huffnagle IM, LiPuma JJ, Huffnagle GB. Comparative genomics of *Pseudomonas fluorescens* subclade III strains from human lungs. *BMC Genomics.* 2015;16:1032.
57. Myers GS, Rasko DA, Cheung JK, Ravel J, Seshadri R, DeBoy RT, Ren Q, Varga J, Awad MM, Brinkac LM, et al. Skewed genomic variability in strains of the toxigenic bacterial pathogen, *Clostridium perfringens*. *Genome Res.* 2006;16:1031–40.
58. Elomari M, Coroler L, Hoste B, Gillis M, Izard D, Leclerc H. DNA relatedness among *Pseudomonas* strains isolated from natural mineral waters and proposal of *Pseudomonas veronii* sp. nov. *Int J Syst Bacteriol.* 1996;46:1138–44.
59. Nakayama K, Kanaya S, Ohnishi M, Terawaki Y, Hayashi T. The complete nucleotide sequence of phi CTX, a cytotoxin-converting phage of *Pseudomonas aeruginosa*: implications for phage evolution and horizontal gene transfer via bacteriophages. *Mol Microbiol.* 1999;31:399–419.
60. Lopez NI, Pettinari MJ, Stackebrandt E, Tribelli PM, Potter M, Steinbuchel A, Mendez BS. *Pseudomonas extremaustralis* sp. nov., a Poly(3-hydroxybutyrate) producer isolated from an antarctic environment. *Curr Microbiol.* 2009;59:514–9.
61. Popoff MR, Bouvet P. Clostridial toxins. *Future Microbiol.* 2009;4:1021–64.

62. Rood JI. Virulence genes of *Clostridium perfringens*. *Annu Rev Microbiol*. 1998;52:333–60.
63. van Asten AJ, Nikolaou GN, Grone A. The occurrence of *cpb2*-toxigenic *Clostridium perfringens* and the possible role of the beta2-toxin in enteric disease of domestic animals, wild animals and humans. *Vet J*. 2010;183:135–40.
64. Freedman JC, Shrestha A, McClane BA. *Clostridium perfringens* enterotoxin: action, genetics, and translational applications. *Toxins*. 2016;8(3):73. doi:10.3390/toxins8030073.
65. Georgiades K, Raoult D. Genomes of the most dangerous epidemic bacteria have a virulence repertoire characterized by fewer genes but more toxin-antitoxin modules. *PLoS One*. 2011;6:e17962.
66. Pandey DP, Gerdes K. Toxin-antitoxin loci are highly abundant in free-living but lost from host-associated prokaryotes. *Nucleic Acids Res*. 2005;33:966–76.

Submit your next manuscript to BioMed Central and we will help you at every step:

- We accept pre-submission inquiries
- Our selector tool helps you to find the most relevant journal
- We provide round the clock customer support
- Convenient online submission
- Thorough peer review
- Inclusion in PubMed and all major indexing services
- Maximum visibility for your research

Submit your manuscript at
www.biomedcentral.com/submit

